A multi-wavelength study of the long-period AM HER system E2003+225-II. Changes in the accretion geometry

Mukai, K.; Bonnet-Bidaud, J.M.; Charles, P.A.; Corbet, R.H.D.; Maraschi, L.; Osborne, J.P.; Smale, A.P.; Treves, A.; van der Klis, M.

DOI
10.1093/mnras/221.4.839

Publication date
1986

Published in
Monthly Notices of the Royal Astronomical Society

Mon. Not. R. astr. Soc. (1986) **221,** 839–856

A multi-wavelength study of the long-period AM Her system E2003+225 – II. Changes in the accretion geometry★

K. Mukai,[1] J.-M. Bonnet-Bidaud,[2] P. A. Charles,[1] R. H. D. Corbet,[1] L. Maraschi,[3] J. P. Osborne,[4,5] A. P. Smale,[1,†] A. Treves,[3] M. van der Klis[6,7] and J. van Paradijs[7]

[1] *Department of Astrophysics, University of Oxford, South Parks Road, Oxford OX1 3RQ*
[2] *CEN-Saclay, Dph/SAP, 91191 Gif-sur-Yvette Cedex, France*
[3] *Dipartimento di Fisica, Università di Milano, Via Celoria 16, 20133 Milano, Italy*
[4] *EXOSAT Observatory, ESOC, Robert Bosch Strasse 5, D-6100 Darmstadt, Federal Republic Germany*
[5] *Affiliated to Astrophysics Division, Space Science Department of ESA*
[6] *Space Science Department of ESA, ESTEC, Postbus 299, 2200 AG Noordwijk, The Netherlands*
[7] *Astronomical Institute 'Anton Pannekoek', University of Amsterdam, Roetersstraat 15, 1018 WB Amsterdam, The Netherlands*

Accepted 1986 March 16. Received 1986 March 13; in original form 1985 December 5

Summary. The longest period AM Her system E2003+225 was observed on 1984 July 24 with *IUE*, with simultaneous optical spectroscopy and photometry from La Palma. The variations of the overall continuum from 1200 to 5000 Å with orbital phase allow a study of the different spectral components in the system. High-resolution optical spectra show complex line profiles containing broad and narrow components. We associate one narrow component with the heated surface of the secondary star, which has enabled us to estimate the parameters of the binary system. E2003+225 has revealed substantial changes compared with the earlier observations; in particular, the large ($\sim$500 km s^{-1}) γ velocity of Nousek *et al.* has decreased to now be consistent with zero velocity.

1 Introduction

We report on a set of observations of the AM Her type object E2003+225 (=QQ Vul; Kholopov *et al.* 1985) carried out in 1984 July using the *International Ultraviolet Explorer* (*IUE*) and two

★Based partly on *IUE* observations collected at the VILSPA station of the European Space Agency.
†Present address: Mullard Space Science Laboratory, Holmbury St Mary, Dorking, Surrey RH5 6NT.

telescopes at the Observatorio del Roque de los Muchachos on La Palma. The observations are presented in Section 2, and the results are discussed in Section 3. A previous set of observations of this object made by this collaboration on 1983 October 12 is described in the accompanying paper (Osborne *et al.* 1986; hereafter Paper I). Throughout this paper, we adopt the new ephemeris, which is introduced in Paper I and refers to the linear polarization pulse.

For a description of AM Her stars, see Paper I, Liebert & Stockman (1985) and references therein. For previous observations of E2003+225, see Nousek *et al.* (1984; hereafter N84).

2 Observations

High time (~2.5 min) and spectral (~1.5 Å) resolution spectroscopy was obtained with the 2.5-m Isaac Newton Telescope (INT) at the Observatorio del Roque de los Muchachos with the RGO spectrograph and Image Photon Counting System (IPCS), covering slightly more than one orbital cycle. Frequent Cu–Ar arc observations were made throughout the observation, and our wavelength calibration is accurate and stable to ~0.1 Å. We also observed the spectrophotometric standard star EG148 (Oke 1974) in order to convert the count rates into fluxes, although conditions at the end of the night were not photometric. The journal of these observations is given in Table 1.

UBVRI photometry was performed with the 1-m Jacobus Kapteyn Telescope (JKT), simultaneously with the spectroscopy and again two nights later. The pass-bands used in the photometer duplicate the *UBV* system of Johnson and the *RI* system of Kron & Cousins (Bessell 1979) with minor differences in the *U* filter (Jones 1984). The observations were made in sequences of *UBVRI–IRVBU*, and the integration time was 8 s for each filter. Due to a telescope problem, only 25 integrations were made in each pass-band on July 24/25; on July 26/27, we were able to make 85 integrations in each (see Table 1).

The *IUE* observations covered two orbital cycles and the second cycle was simultaneous with the optical spectroscopic observations. Short exposure times were chosen so as to study

Table 1. Journal of observations.

	Date	Exposure	Time	Cycle/Phase
INT*	24/25 July		2251 UT - 0307 UT	1.45 - 2.60
JKT**	24/25 July		0148 UT - 0346 UT	2.29 - 2.82
JKT***	26/27 July		2218 UT - 0441 UT	0.30 - 2.01
IUE	24/25 July	LWP 3856	1926 UT - 1946 UT	0.53 - 0.62
		SWP 23503	1953 UT - 2039 UT	0.65 - 0.85
		LWP 3857	2043 UT - 2103 UT	0.87 - 0.96
		SWP 23504	2110 UT - 2155 UT	0.99 - 1.19
		LWP 3858	2159 UT - 2219 UT	1.21 - 1.30
		SWP 23505	2230 UT - 2310 UT	1.35 - 1.53
		LWP 3859	2314 UT - 2334 UT	1.55 - 1.64
		SWP 23506	2343 UT - 0023 UT	1.68 - 1.86
		LWP 3860	0028 UT - 0048 UT	1.88 - 1.97
		SWP 23507	0056 UT - 0136 UT	2.01 - 2.19
		LWP 3861	0142 UT - 0202 UT	2.22 - 2.31
		SWP 23508	0208 UT - 0248 UT	2.33 - 2.51

*80 exposures (the integration times are usually 100 seconds).
**25 integrations in each passband, with 8 second integrations.
***85 integrations in each.

phase-related changes in the UV spectrum. Six spectra were obtained with the short-wavelength camera (SWP; 1200–1950 Å) alternating with six long-wavelength spectra (LWP; 1900–3100 Å).

2.1 PHOTOMETRY

The light curves folded on the orbital period of E2003+225 in five colours are plotted in Fig. 1. The data taken on July 24/25 are not included in this figure, because there are insufficient data points to significantly improve the figure and the weather was not ideal. The light curves obtained on the two nights are similar, with possible minor differences which may be attributed to the weather. We observed two minima per cycle in the optical: the principal minimum is centred

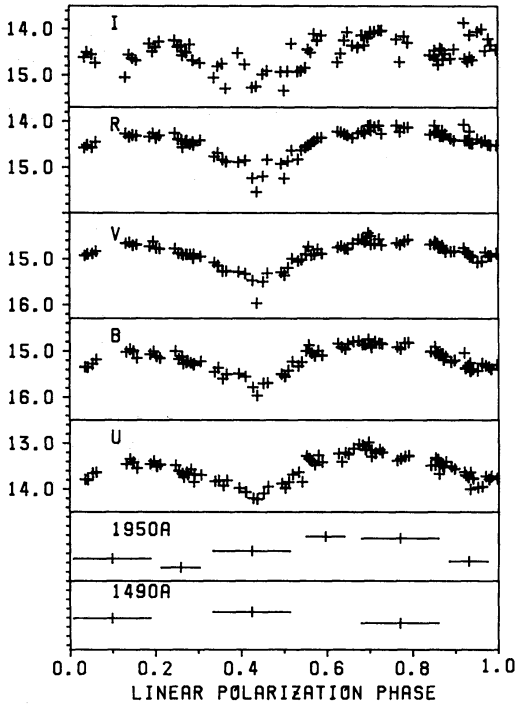

Figure 1. Five-colour photometry obtained on 1984 July 26 with JKT folded on the orbital period. UV 'magnitudes' at 1950 and 1490 Å are also shown.

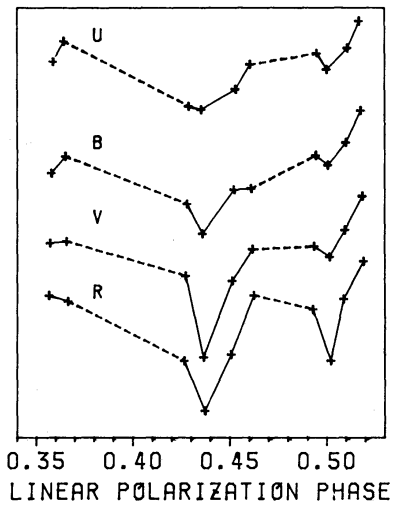

Figure 2. Sharp dips observed on 1984 July 26. The vertical scale is the relative change in magnitudes. The dotted lines indicate the intervals when the sky and comparison star measurements were made.

around $\phi \sim 0.44$ and has a width in phase of ~ 0.15 in B; the secondary minimum is centred around $\phi \sim 0.0$. This result is somewhat different from N84 light curves; particularly, the depths of the minima and their colour dependence have changed. We do not see the spectacular ~ 1.5 mag drop in the U band seen by N84 (their fig. 11); the depth in our data is ~ 0.7 mag.

Within the principal minimum, two sharp dips are visible, one at $\phi \sim 0.43$ and another at $\phi \sim 0.50$ (Fig. 2). The V magnitude, which has an average of ~ 15.5 during the principal minimum outside the dips dropped to 15.95 during the dip at $\phi \sim 0.43$; R dropped from 14.85 to 15.55, while the dip is less prominent in B and U. Although flickering activities, with time-scales of several minutes, are seen throughout our observations, the typical amplitudes are ~ 0.1 mag and clearly do not explain this dip. The total width of this dip is about 5 min, and the 'colour dependence' may be due to a very sharp (~ 1 min) central dip at the time of the V and R observations. This feature is very similar to that noted in the N84 blue light curve at $\phi \sim 0.38$.

For the purpose of comparison, we have extracted the mean blue light curve from N84, and plot this in Fig. 3 together with our B light curve and the spectroscopic B light curve of 1983 October (Paper I).

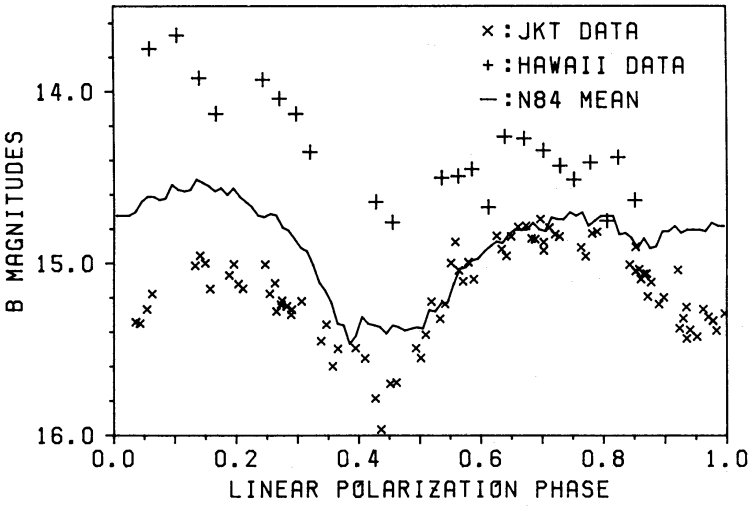

Figure 3. *B* light curve from N84, Hawaii spectrophotometry (Paper I), and JKT data.

2.2 UV/OPTICAL CONTINUUM

The six SWP spectra are plotted in Fig. 4. It is clear that both the continuum (see also Fig. 1 and Table 2) and emission lines are variable and this variability is associated with phase (since spectra taken at the same phase are similar). The average intensity is similar to that of 1983 October (Paper I).

We investigated the UV continuum by fitting both a power law and a blackbody to the line-free regions of the six SWP and six LWP spectra. The fluxes at selected wavelengths are reported in Table 2; at 1950 Å, which falls at the extremes of both the short- and the long-wavelength ranges, the fluxes were derived using the best-fit power laws. They are then converted into 'magnitudes' and included in Fig. 1 together with the optical light curves. From all the combinations of successive SWP and LWP, eight are selected whose fluxes are similar at 1950 Å (derived as above), and the continuum of the combined SWP/LWP spectra are fit with a power law and blackbody. We report the χ^2_ν and spectral indices and temperatures of the best fit (together with the errors on the last digit) in Table 2. The power law is found to be a somewhat better fit than the blackbody.

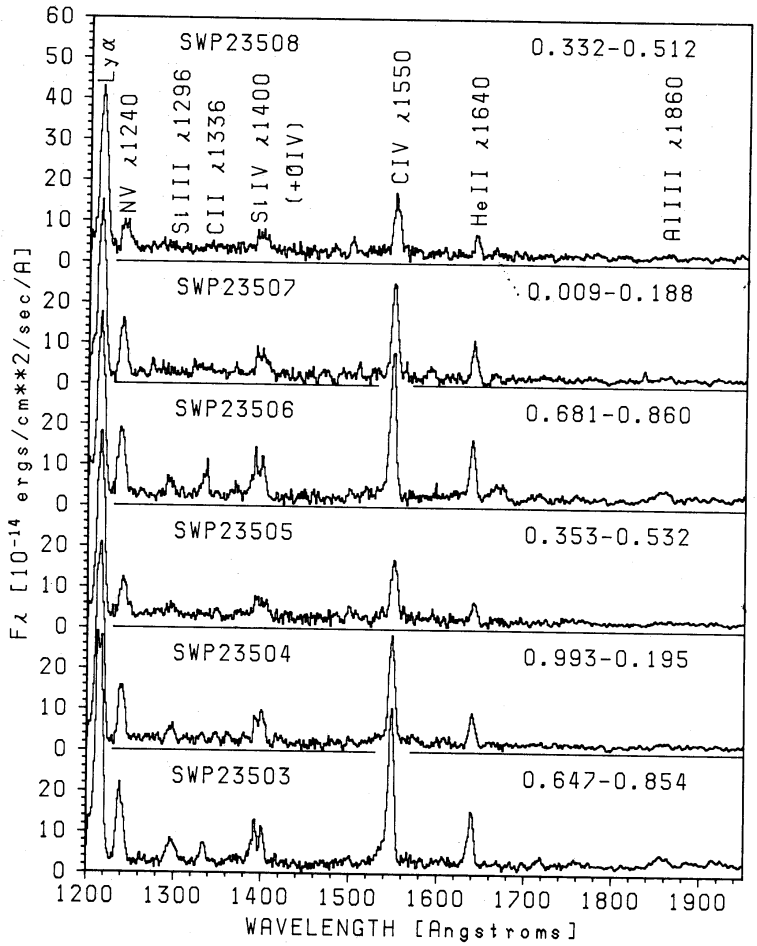

Figure 4. The six *IUE* SWP spectra are plotted. Time goes from bottom to top. The panels are not clearly separated at Lyα (contaminated by geocoronal emission) and C IV λ1550 (*not* contaminated).

Table 2. UV continuum of E2003+225.

		Flux (10^{-14} ergs cm^{-2} s^{-1} Å^{-1})				Power Law Fit		Blackbody Fit	
Exposure	Phase	1490Å	1780Å	1950Å	2725Å	χ^2_ν	α	χ^2_ν	T(10^3K)
LWP 3856	0.53 - 0.62			3.1	1.8				
SWP 23503	0.65 - 0.85	2.8	3.0	3.0		15.2	-0.60(3)	10.5	6.0(1)
LWP 3857	0.87 - 0.96			2.1	1.2				
SWP 23504	0.99 - 0.19	3.0	2.1	1.9		6.1	-0.75(4)	14.4	16.8(2)
LWP 3858	0.21 - 0.30			1.7	1.2	5.4	-0.86(4)	12.5	17.1(2)
SWP 23505	0.35 - 0.53	3.4	2.4	2.2		5.0	-1.17(0)	11.2	19.2(2)
LWP 3859	0.55 - 0.64			3.1	2.0				
SWP 23506	0.68 - 0.86	2.7	2.6	2.8		7.2	-0.38(3)	9.2	14.9(1)
LWP 3860	0.88 - 0.97			1.8	1.3				
SWP 23507	0.01 - 0.19	3.0	2.1	1.9		3.2	-0.95(4)	9.4	17.2(2)
LWP 3861	0.22 - 0.31			1.6	1.2	4.8	-0.89(4)	11.2	17.1(2)
SWP 23508	0.33 - 0.51	3.4	2.1	2.0		4.6	-1.12(3)	13.9	18.8(2)

The amplitude of the modulation in the far-UV is comparable to that in the *B* band. However, while the maximum in the far-UV at $\phi\sim0.6$–0.8 is coincident with that in the optical, the minimum in the far-UV is at $\phi\sim0.2$–0.3, not at $\phi\sim0.45$ as is the case in the optical. A possible interpretation of this phenomenon will be discussed in Section 3.1.

From Table 2 and Fig. 1 it is also clear that there are significant phase-related variations in the shape of the UV continuum (see also Fig. 6). At $\phi=0.65$–0.85 it is much redder than at other phases. In fact the data indicate that, at very short wavelengths ($\lesssim$1500 Å), the intensity variation is reversed with respect to longer wavelengths, the minimum occurring at $\phi\sim0.77$ while the maximum occurs at $\phi\sim0.42$.

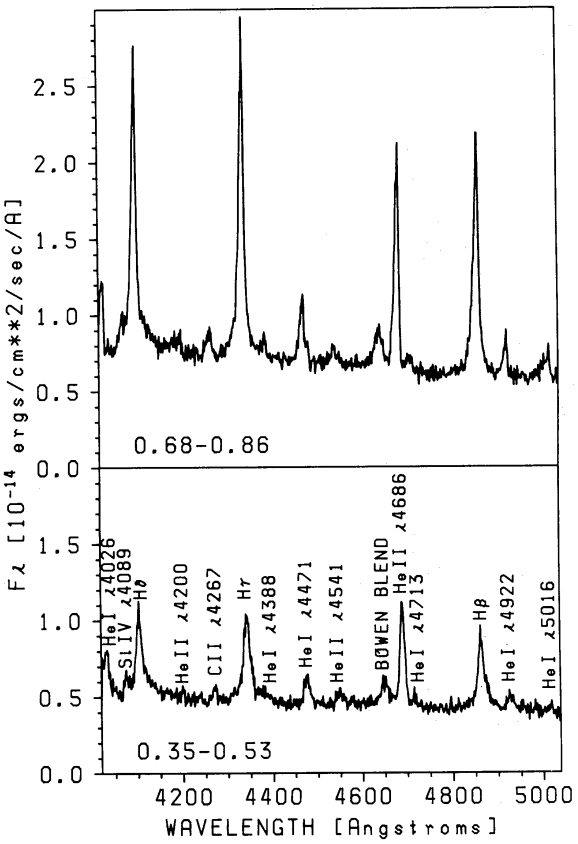

Figure 5. Average spectra from INT observations at two representative phases.

Optical spectra at different phases are shown in Fig. 5. Also in the optical–IR range, the continuum is redder at $\phi\sim0.77$, i.e. at maximum intensity, as derived from photometric and spectrophotometric data.

The combination of optical and UV continua taken at phases centred at 0.77 and 0.42 are shown in Fig. 6, together with the power-law and blackbody best fits. The two extreme soft X-ray blackbody curves allowed by the 1983 October *EXOSAT* grating observation (Paper I) are extrapolated to the UV and plotted for comparison. The average of *UBVRI* magnitudes for the same phase intervals are also plotted in Fig. 6. The *B* point in the upper panel (optical maximum) is well above the continuum points, but can be explained by the extremely strong emission lines at that particular phase (see Fig. 5). We calculated the contribution of emission lines in the maximum and minimum, by folding (i) an interpolated continuum and (ii) the spectrum as observed through the standard filter response. These are compared with (iii) the average *B*

magnitude from our broad band photometry from the same phase interval. We obtain (i) 15.27 (ii) 14.63 and (iii) 14.62 for the optical maximum ($\phi \sim 0.68$–0.86), and (i) 15.46 (ii) 15.16 and (iii) 15.14 for the minimum ($\phi \sim 0.35$–0.53). This is the cause of the apparent discrepancy between the spectroscopic and photometric points in the upper panel of Fig. 6. The *U* point is also above the best-fit power law during optical maximum and not during the minimum; the excess flux, $\sim 4.3 \times 10^{-12}$ erg cm^{-2} s^{-1} can be explained as due to the strong Balmer continuum from the emission-line region.

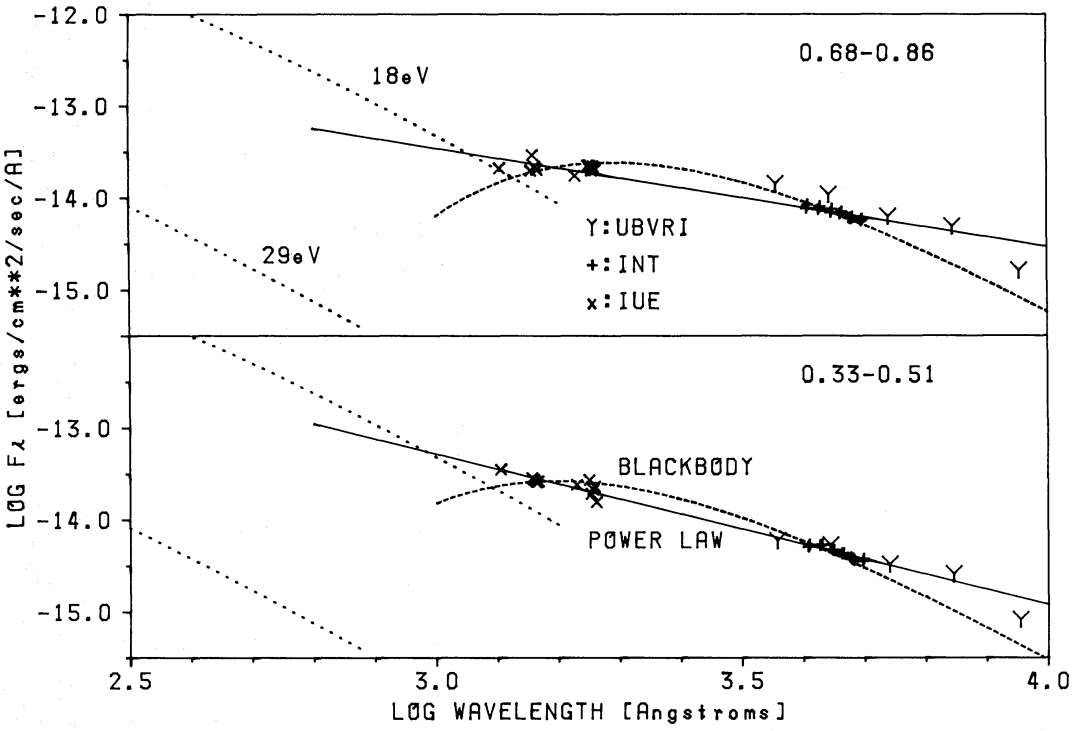

Figure 6. The SWP and optical continuum are plotted with the best power-law fits and the best blackbody fits for the two phases. The spectral indices and the temperature are $\alpha = 1.28$ and $T = 15\,000$ K, and $\alpha = 1.59$ and $T = 18\,500$ K for the upper and lower panel, respectively. The extrapolation of the two extreme cases of soft X-ray blackbody fits (from 1983 October observation, see Paper I) are also plotted.

2.3 THE EMISSION LINES

The emission lines observed both in the optical and UV are typical of AM Her stars (e.g. Liebert & Stockman 1985).

Although a complex structure in the optical emission lines can clearly be seen, for comparison with previous lower resolution observations, we have smoothed our data into 4 Å bins to simulate the effect of lower resolution. We then fitted a Gaussian profile to each of the four strongest emission lines in the region: Hβ, He II λ4686, Hγ and Hδ. The velocity of Hβ in our data and in the Mauna Kea observation of 1983 October 12 (Paper I) and the best-fit sinusoid of N84 are plotted in Fig. 7. A striking difference in the orbital average of the radial velocity (γ) is apparent; this change in γ is discussed in Section 3.2 below. The parameters of the best-fitting sinusoids are reported in Table 3.

The equivalent widths of Hβ, He II λ4686, He I λ4471 and the Bowen blend are plotted in Fig. 8. The equivalent width of Hβ has a broad maximum around $\phi = 0.7$, and there is a sharp eclipse at $\phi \sim 0.47$; this behaviour is also seen in other Balmer lines, although the eclipse is less prominent in

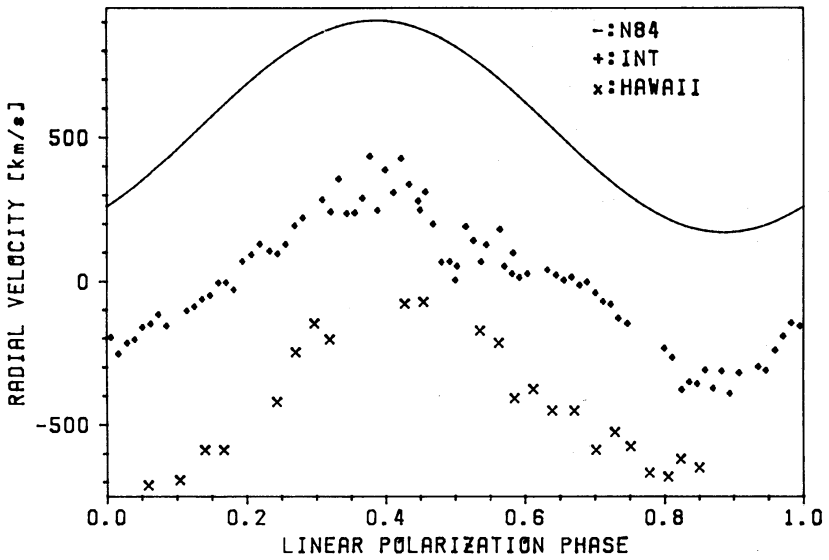

Figure 7. Radial-velocity curves of Hβ from N84, Hawaii data (Paper I) and INT.

Table 3. E2003+225 line velocities. Best-fit parameters to $V=\gamma+k\sin[2\pi(\phi-\phi_0)]$.

Lines	γ (km s^{-1})	K (km s^{-1})	ϕ_0
Hβ	-15.6±9.9	289.4±16.2	0.138±0.007
HeII λ4686	-21.6±7.6	339.5±11.9	0.128±0.005
Hγ	-16.6±10.2	308.6±15.9	0.125±0.007
Hδ	6.5±9.9	315.8±18.0	0.131±0.007
NV λ1240		407±57	0.120±0.017
CIV λ1550		246±48	0.150±0.023
HeII λ1640		277±74	0.120±0.035

Hγ and Hδ. He I λ4471 may also have a similar phase dependence, although the evidence for this line in itself is not strong enough. He II λ4686, on the other hand, is almost constant throughout the orbital cycle, except for a short eclipse at $\phi\sim0.49$. The Bowen blend is also constant. This overall behaviour is similar to that observed in 1983 October (Paper I). However, we do not see a He II eclipse in the 1983 data.

Strong changes in the UV emission lines are apparent in Fig. 4, with evidence of correlation

Table 4. Equivalent widths (Å) and fluxes (10^{-14} erg cm^{-2} s^{-1}) of UV emission lines.

	SWP 23503		SWP 23504		SWP 23505		SWP 23506		SWP 23507		SWP 23508	
Line	E.W.	I.	E.W	I.	E.W.	I.	E.W.	I.	E.W.	I.	E.W.	I.
NV λ1240	83	238	51	160	27	133	74	203	46	157	18	120
SiIV+OIV λ1400	51	188	35	122	28	141	49	186	29	114	20	99
CIV λ1550	130	432	140	320	49	171	120	382	96	240	51	153
HeII λ1640	38	155	31	88	11	60	43	168	28	87	13	61

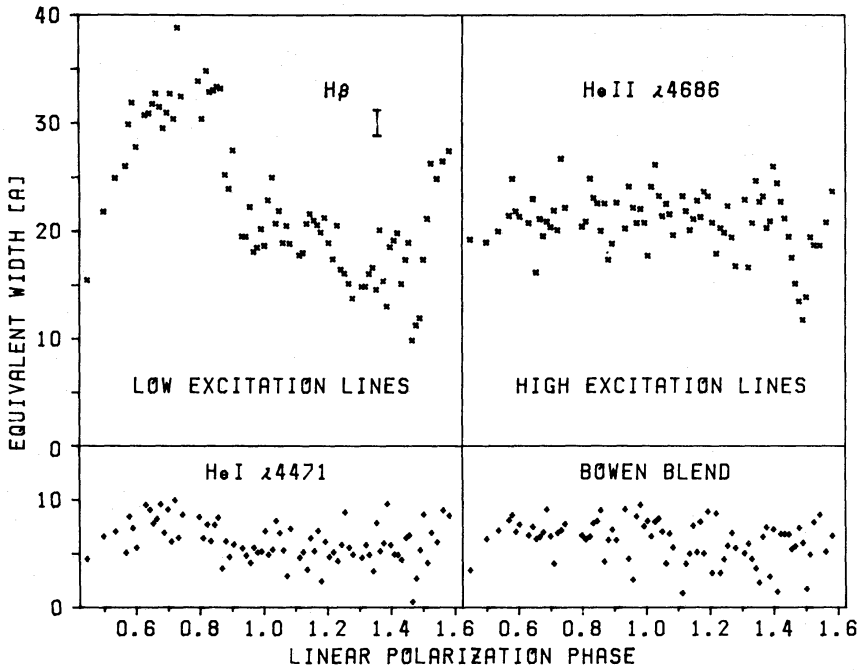

Figure 8. Equivalent-width variation of Hβ, He I λ4471, He II λ4686 and the Bowen blend in the INT data.

with orbital phase. The equivalent width and the intensity of the prominent lines are given in Table 4. The lines appear strongest when the optical and UV continuum is brightest. The equivalent width of all the prominent UV lines, i.e. N V, Si IV, C IV, He II, show clear maxima at $\phi \sim 0.75$, a behaviour similar to the Balmer lines. The line profiles of the three prominent UV emission lines, N V λ1240, C IV λ1550 and He II λ1640, were fitted using single Gaussians, which reveal a radial-velocity variation (Fig. 9). We then performed a sinusoidal fit using a fixed period,

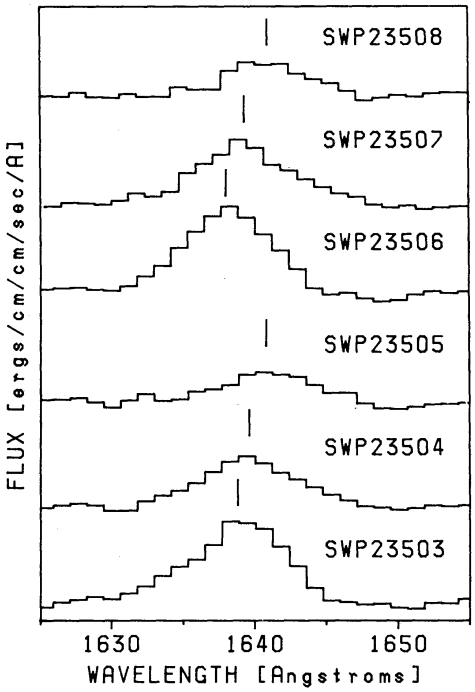

Figure 9. The profiles of He II λ1640 lines from the six SWP spectra are plotted. The tick marks show the measured position of the line, and are used in the sinusoidal fit.

and the best-fit parameters are reported in Table 3. Although the velocity differences detected (up to ~2 Å) are small compared to the resolution of *IUE* (≤7 Å; Boggess *et al.* 1978) the similarity of these parameters to those of the optical emission lines argues for the reality of this radial-velocity variation. The accuracy of the absolute wavelength calibration of the *IUE* data prevents us from stating the γ-velocity of these lines.

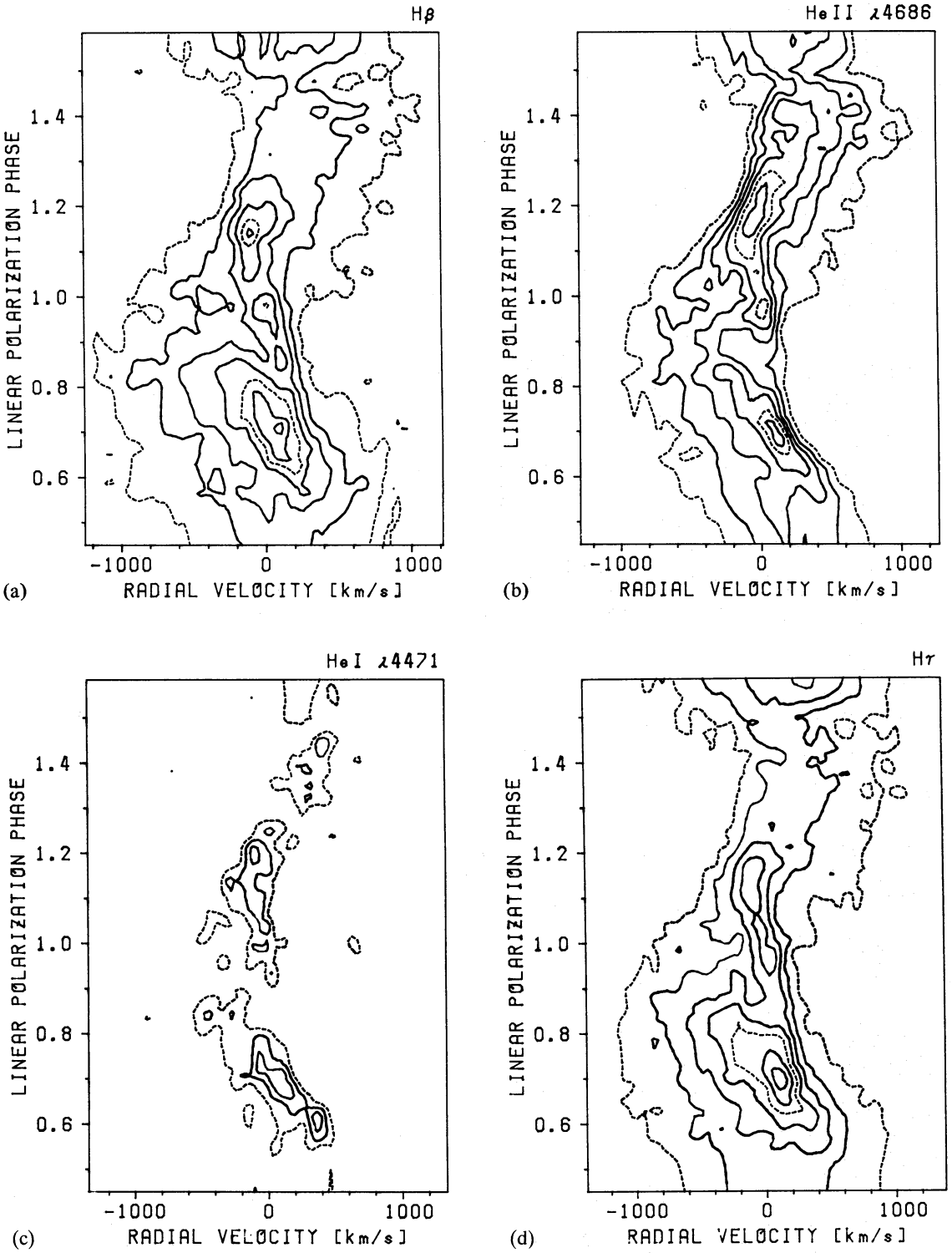

Figure 10. Contour plots of the intensities of four emission lines (Hβ, He IIλ4686, He Iλ4451 and Hγ). The levels are 1.5, 2.0, 2.5, 3.0, 3.5, 4.0 and 4.5 times the continuum.

The high spectral resolution of our INT data enables the complex time-varying structure of the emission lines to be presented in the form of intensity contour plots in the velocity-time plane (Fig. 10). This can be compared to similar analyses for other AM Her stars. The profiles are characterized by a broad base with sharp components superposed (see examples in Fig. 11), which is typical of AM Her like objects, and EF Eri in particular (see Mukai & Charles 1985 and references therein).

The technique of measuring the line positions varies from one author to another, and sometimes even the same author(s) may use different methods. Here we have adopted a multiple-Gaussian fitting procedure; although there is no *a priori* reason to assume Gaussian profiles for the broad component, for which the broadening mechanism is not known, the 'base' and the 'peak' of the broad component can be reasonably represented by single Gaussians. We do not know whether these represent two different regions within the gas stream or are just convenient approximations of a single, asymmetric component. The actual fitting proceeded as follows: first, the central portion of the emission line was excluded and a single Gaussian was fitted, giving the velocity for the base of the broad component. Then the parameters of the base component were fixed, and a fit with multiple peaks was performed to the entire data, giving the velocities of the peaks. In this way, a series of velocities were obtained for the base and multiple peaks. Because we found no systematic difference between the velocities of various lines (which is not always the case in AM Her type objects), we assembled the velocity data from all the lines and plotted them in Fig. 12.

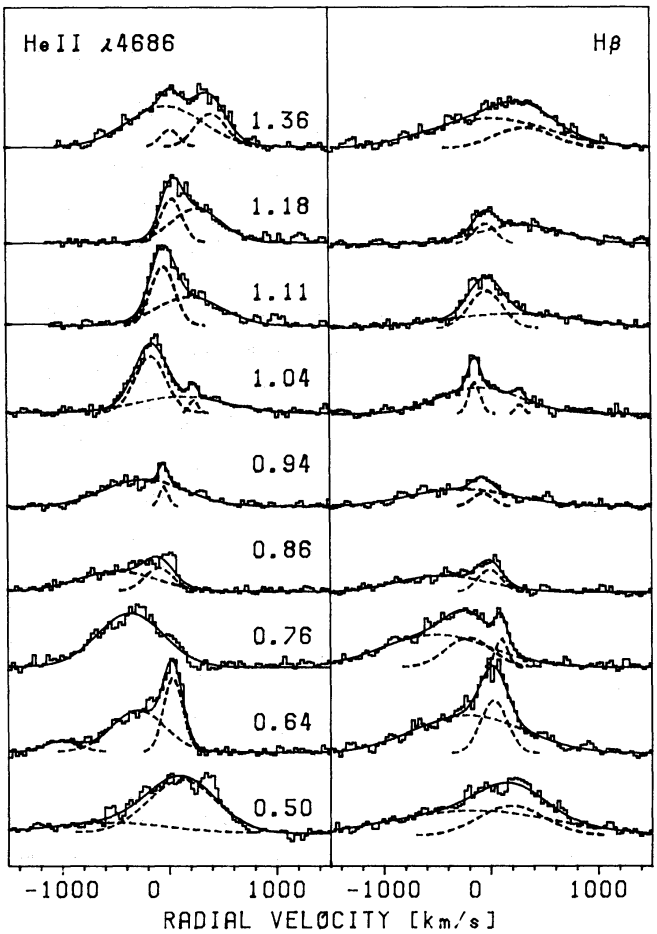

Figure 11. Examples of the multi-component fits to Hβ and He II λ4686. The histograms represent the data points, the solid lines are the combined best fits and the dotted lines are the individual components of the fits.

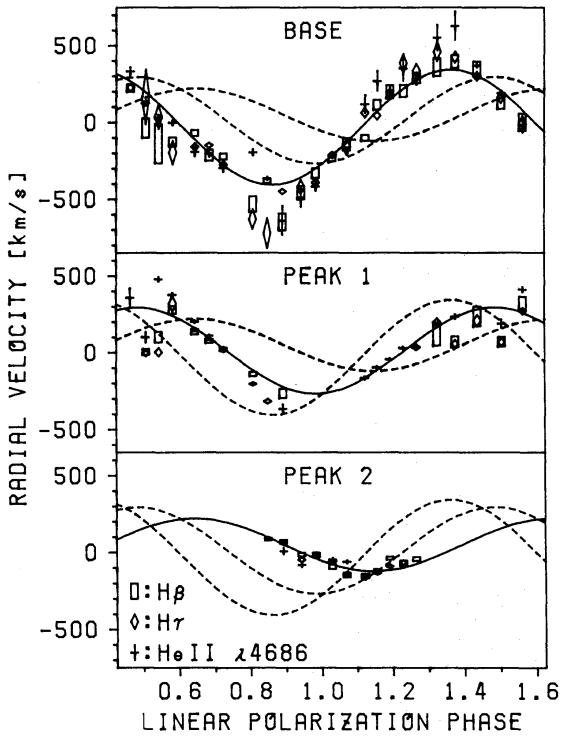

Figure 12. Radial-velocity curves of the various components in the Balmer lines and He II λ4686.

A sinusoidal fit was performed to the velocities of the base component; it essentially coincides with that obtained by degrading the spectral resolution. This is plotted in Fig. 12. We find another sinusoid, connecting many of the peaks, which lags the base component by $\Delta\phi\sim0.1$; these two components probably originate in a slightly different location in the accretion flow and the velocity is dominated by the infalling motion (see Section 3.2). The curvature of the column and the distribution of velocity can produce asymmetric profiles which are reasonably represented by a combination of two Gaussians.

There is another series of peaks, often sharper than the others, and out of phase with the broad component. This component can be associated with the heated surface of the secondary (see Biermann *et al.* 1985 for a discussion of the sharp component). The corresponding velocity curve is also given in Fig. 12. This component has a γ velocity of $50\,\mathrm{km\,s^{-1}}$, semi-amplitude of $170\,\mathrm{km\,s^{-1}}$, and the phase of velocity crossing gamma from blue to red is found to be ~0.4, although these values have considerably larger errors than those for the base component, due to the shortness of its appearance. This information can be used to determine the parameters of the system.

2.4 THE SYSTEM PARAMETERS

We follow the approach of Patterson (1984) and assume that the secondary is a main-sequence star, satisfying the empirical ZAMS mass–radius relationship,

$$R_s=M_s^{0.88}, \tag{1}$$

where R_s and M_s are the secondary star radius in solar radii and mass in solar masses, respectively. Then the orbital period, Kepler's third law and an approximate expression for the Roche geometry are sufficient to yield

$$R_s=0.40\,R_\odot \tag{2}$$

$$M_s=0.35\,M_\odot. \tag{3}$$

If we allow for a slight (10 per cent) departure of the mass–radius relation from equation (1), we find the expected spectral type of the secondary to be M2–4V.

Now we can use the sharp component to restrict the mass ratio, q, ($=M_s/M_w$, where M_w is the mass of the white dwarf). However, the ordinary method of estimating the mass function has to be modified, since the R_s is comparable to a, the binary separation. Thus, if the sharp component of the emission lines is coming from the L_1 point, the distance between the L_1 point and the centre of mass of the secondary (R_{L_1}) must be subtracted from $a/1+q$. In a more realistic model, the sharp emission lines come from an extended region on the surface of the secondary, where the distance from the centre of mass of the binary system is greater than at the L_1 point. If we write the effective radius of the secondary to be subtracted, averaged over this sharp emission-line region, as R'_s, then we find

$$\left(\frac{a}{1+q}-R'_s\right)\frac{2\pi}{P}\sin i=8.23\times10^{-4}K_s, \tag{4}$$

where i is the inclination of the system, K_s is the semi-amplitude of the sharp component (km s^{-1}), and P is the period (hr). R_{L_1} is greater than R_s, which is the volume-averaged radius of the secondary; on the other hand, inclusion of an extended region tends to reduce the effective radius. Taking both factors into account, we assume $R'_s \sim R_s$. Equation (4) and Chandrasekhar's limit then leads to

$$0.24 \lesssim q \lesssim 0.40. \tag{5}$$

If we assume $i=60°$, consistent with the polarization measurements of N84, we find

$$q=0.35 \tag{6}$$

$$M_w \sim 1.0\,M_\odot \tag{7}$$

$$a \sim 1.3\,R_\odot. \tag{8}$$

From the spectral type of the secondary and the observed I magnitude at the broad minimum, we can place a lower limit to the distance to E2003+225. Assuming a secondary spectral type of M4V, the faintest within the range derived above, yields an absolute I magnitude of 9.11 (Young & Schneider 1981). Combined with the observed value of I during minimum (~15.0), the distance to the system must exceed 150 pc.

3 Discussion

3.1 LIGHT CURVE

A schematic diagram of the E2003+225 system is shown in Fig. 13, using the parameters deduced in the previous section. In Fig. 14, we plot the X-ray light curve of 1983 October (Paper I), the B light curve, Hβ equivalent width and radial velocity as a function of phase. Note that there is a distinct possibility that the phase of various events shifted between 1983 October and 1984 July. The O–C scatter of the linear polarization pulses are large (up to ~4 per cent; see table 1 in Paper I), and we do not have enough observational data to determine if there has been any shift in the optical light curve, for example.

The broad minimum in the optical light curve, centred at $\phi \sim 0.44$, is broader than the X-ray minimum, as is evident in Fig. 14. The optical minimum is probably caused by a combination of cyclotron beaming (Liebert *et al.* 1982) and the occultation of the inner part of the accretion column by its outer part, as discussed in Paper I. However, it is not clear how this relates to the earlier soft X-ray light curve.

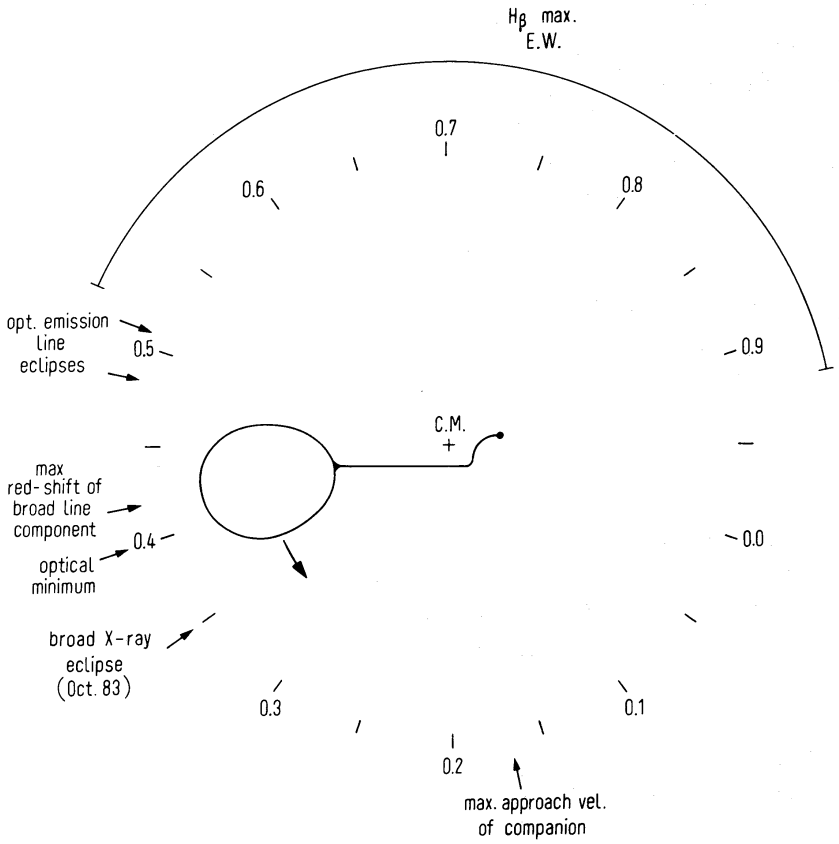

Figure 13. The schematic diagram of the system geometry.

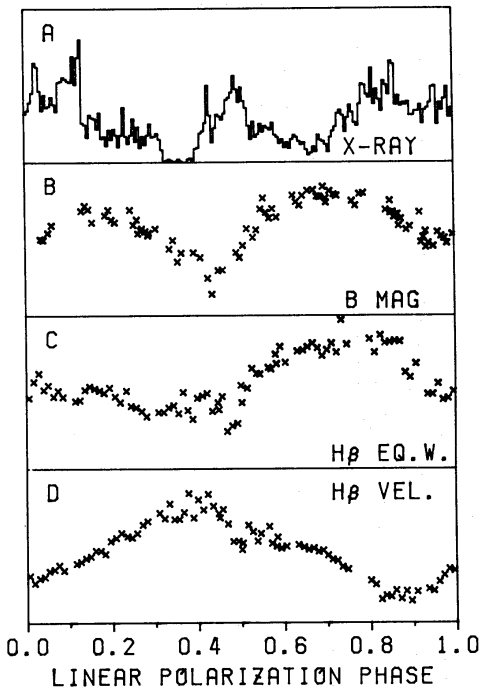

Figure 14. (a) The soft X-ray light curve (Paper I) (b) the *B* band light curve; (c) the equivalent width of Hβ and (d) the radial velocity of Hβ are plotted against linear polarization phase.

Sources of light other than cyclotron radiation may contribute in the optical/UV region. The fact that the amplitude of the modulation in U is larger than that in the I band, where the cyclotron component is expected to be strongest, shows that a second source of radiation varies with the same phasing as the cyclotron component. We suggest that this component is thermal continuum from the accretion column near the emission-line region. The soft X-ray and EUV photons and the cyclotron radiation from the shock region would suffice as the heating mechanism. The plasma above the shock may be optically thick so that the varying aspect of the emission region could be responsible for the modulation. If the region is cylindrical with length larger than the radius, the behaviour of the U light curve could be roughly explained.

The simultaneous optical and UV spectra taken at $\phi \sim 0.75$, where both the cyclotron and the thermal emission from the accretion column are at maximum (see Fig. 6) suggest that the temperature of the gas is $\sim 15\,000$ K.

The different phase dependence of the emission at the highest UV frequencies suggests that a third hotter component is present which is stronger when the line-of-sight is nearly parallel to the column. This may be associated with the hot polar cap which produces soft X-rays. The spectrum of this hotspot UV component is rather uncertain, taking into account that even at $\phi \sim 0.4$ the cyclotron and thermal radiation from the column are still important at long wavelengths. However, it is interesting to note that in three AM Her type systems, AM Her (Raymond *et al.* 1979), E1405−451 (Maraschi *et al.* 1984) and PG1550+191 (Szkody, Liebert & Panek 1985), a λ^{-4} component has been detected in the short-wavelength UV.

A comparison with the blackbody fits to the X-ray spectrum obtained in 1983 October (Paper I) indicates that the UV flux is in excess of the extrapolated soft X-ray emission (Fig. 6). This is also the case with AM Her, where the blackbody spectrum determined by the *Einstein* OGS observation (Heise *et al.* 1984) does not explain the λ^{-4} component. A natural explanation is that the polar cap is characterized by a temperature distribution rather than a single temperature. The innermost hot region would dominate in soft X-rays whereas a cooler outer region would contribute mainly in the UV. If this outer region is significantly larger than the central part of the hotspot and the accretion column near the shock, then one could account for the fact that absorption in the column causes the X-ray and optical minima while not affecting the far-UV.

3.2 THE BROAD EMISSION LINES

In this section, we address the problem of the origin of the broad emission lines with particular emphasis on their γ-velocity.

It is generally believed that the accreting stream near the white dwarf is responsible for the broad component of the emission lines (e.g. Liebert & Stockman 1985). In fact, using the parameters derived for E2003+225, the Keplerian motion of the white dwarf is of the order of $100\ \mathrm{km\ s^{-1}}$, and the observed radial velocities are therefore dominated by the infalling motion of the gas.

Let us now consider the emission from a point in the stream. We define the z axis to be perpendicular to the orbital plane with the Earth in the $z>0$ half-space, and separate the velocity into two components, $V_{\parallel}$ (parallel to the orbital plane) and V_z (the z component). The radial velocity we observe is the projection of this velocity vector into our line-of-sight. The z component of the line-of-sight vector stays constant as we move around the system, whereas the component parallel to the orbital plane is modulated. Therefore, the γ we observe is $-V_z \cos i$. The fact that we observed a negative (although close to zero) γ in 1984 July indicates that, at the time, the emission lines originated in a region where the gas is leaving the orbital plane, rather than falling toward it.

This is also consistent with the lower limit of the distance to the white dwarf surface derived

from the fact that our spectra do not display Zeeman splitting in the emission lines. Although the complex profile makes it difficult to detect any such splitting in one of the components, the surface magnetic field of ~20 MG, a typical value for AM Her systems (Liebert & Stockman 1985), would imply a huge shift (~320 Å) for the σ^- component of Hβ, if the emission originated at the white dwarf surface. Assuming an r^{-3} variation in the strength of the magnetic field and setting an upper limit of ~5 Å on any splitting in the lines we can conclude that the broad emission-line region is at least ~2.5 white dwarf radii away from the surface. It should be noted that, under the assumption of free fall, a velocity of ~1000 km s^{-1} will occur in a region $\sim 3\times10^{10}$ cm from the surface, which is consistent with the magnetospheric radius of Liebert & Stockman (1985). However, given the interaction of the stream with the magnetosphere (see e.g. Lamb 1985) this assumption is uncertain.

As shown in Fig. 7, several remarkable changes in γ have occurred. In 1983 October, γ changed from a value close to zero (Lick observations) to a large negative value (Mauna Kea observations) within a few hours (Paper I). Optical spectroscopy performed in 1984 June shows γ to be consistent with zero (McCarthy, Clarke & Bowyer 1985), which is consistent with our INT spectroscopy.

This series of changes can be explained, at least qualitatively, in the context of the model considered above. In 1982 September (N84) and in 1983 October (Paper I), the bulk of the emission lines originated very near the white dwarf, where V_z is negative. In 1984 July, the emission-line region has moved away from the white dwarf, where $V_z \gtrsim 0$, and hence we would observe $\gamma \lesssim 0$. The semi-amplitude would not be affected much by such a change because the velocity of the gas is already high when it is turned around by the magnetic field. This change of location could be due to a change in the accretion rate, but we did not find any clear evidence for a correlated change in the optical, UV or X-ray luminosities.

In addition to the change in the radial-velocity curves, one major problem remains, namely the equivalent-width variation over the orbital cycle. The Balmer and UV lines vary with orbital phase, in both equivalent width and intensity, with a broad maximum at 0.6–0.9 (see Table 4 and Fig. 8). A possible interpretation is that these lines originate from a region optically thick to the lines, and that the modulation is related to the varying aspect of the region. This is supported by the observed inverted Balmer decrement, which is present in all AM Her systems, implying a high density of the emission region (e.g. Liebert & Stockman 1985). On the other hand the equivalent width of He II λ4686 stays roughly constant through the orbital cycle, indicating that the region should be optically thin to this line.

From the simultaneous optical and UV observations we can derive line ratios for four He II lines (Table 5). A comparison with 'case B' values (Brocklehurst 1971; Seaton 1978) shows significant disagreement, although He II λ2733 may well be heavily contaminated by the N III Bowen lines. Specific calculations for optical depths larger than assumed in case *B* consistent with the proposed interpretation would be needed to discuss this point further.

Table 5. Fluxes of He II $\lambda\lambda$1640, 2734 and 4541 normalized to λ4686 (=100).

	SWP 23505	LWP 3859	SWP 23506	LWP 3860	SWP 23507	LWP 3861	SWP 23508	COMPUTED (Case B)
λ1640	1149		1148		525		680	560
λ2734		485		279		155		17
λ4541	13.0	18.6	11.4	10.3	13.3	13.8	17.7	3.5

3.3 LONG-TERM BEHAVIOUR OF E2003+225

The accumulated observations of this system at various wavelengths have revealed several remarkable changes. These are:

(i) The change in the systemic velocity (γ), as discussed in Section 4.2.

(ii) The optical light curve has changed: as reported in Section 3.1, our light curve is different to that of N84. The light curve derived from the spectrophotometry at Mauna Kea (Paper I), although it covers less than an orbital cycle and has several gaps in it, shows a behaviour different from either of them (see Fig. 5).

(iii) A change in the eclipse behaviour of the emission lines: the variation of the equivalent width of Hβ and He II λ4686 with time (Fig. 8) reveals an emission-line eclipse at $\phi \sim 0.53$, while a similar plot for our Mauna Kea spectroscopy (Fig. 8 of Paper I) shows an eclipse of Hβ only and not of He II λ4686. This indicates either that λ4686 was not eclipsed or that a λ4686 eclipse did occur, but at a different phase.

Through our simultaneous and quasi-simultaneous observations at various wavelengths, E2003+225 has been shown to be a very complex system which undergoes both short-term and long-term changes in its accretion geometry. As the longest period AM Her system, we believe it offers an excellent laboratory for furthering our understanding of the evolution of magnetic cataclysmic variables.

Acknowledgments

The INT and the JKT, on the island of La Palma, are operated by the Royal Greenwich Observatory at the Spanish Observatorio del Roque de los Muchachos of the Instituto de Astrofisica de Canarias. The observations with these two telescopes in the early stage of their operation were made possible by the remarkable efforts of the staff. We particularly thank Bob Fosbury and Derek Jones, our support astronomers, and V. Reyes, our night assistant. We thank the authors of N84, in particular John Nousek and Howard Bond, for communicating the details concerning their observations. We also thank John Nousek for sending materials prior to publication, and for some useful discussions. One of us (KM) is a recipient of an Overseas Research Scholarship. APS acknowledges an SERC studentship.

References

Bessell, M. S., 1979. *Publs astr. Soc. Pacif.*, **91,** 589.

Biermann, P., Schmidt, G. D., Liebert, J., Stockman, H. S., Tapia, S., Kühr, H., Strittmatter, P. A., West, S. & Lamb, D. Q., 1985. *Astrophys. J.*, **293,** 303.

Boggess, A. *et al.*, 1978. *Nature,* **275,** 377.

Brocklehurst, M., 1971. *Mon. Not. R. astr. Soc.*, **153,** 471.

Heise, J., Kruszewski, A., Chlebowski, T., Mewe, R., Kahn, S. & Seward, F. D., 1984. *Phys. Scripta,* **T7,** 115.

Jones, D., 1984. *RGO/La Palma Technical Note No. 10.*

Kholopov, P. N., Samus', N. N., Kazarovets, E. V. & Perova, N. B., 1985. *Inf. Bull. Var. Stars No. 2681.*

Lamb, D. Q., 1985. In: *Cataclysmic Variables and Low-Mass X-ray Binaries,* p. 179, eds Lamb, D. Q. & Patterson, J., Reidel, Dordrecht, Holland.

Liebert, J. & Stockman, H. S., 1985. In: *Cataclysmic Variables and Low-Mass X-ray Binaries*, p. 151, eds Lamb, D. Q. & Patterson, J., Reidel, Dordrecht, Holland.

Liebert, J., Stockman, H. S., Williams, R. E., Tapia, S., Green, R. F., Rautenkranz, D., Ferguson, D. H. & Szkody, P., 1982. *Astrophys. J.*, **256,** 594.

McCarthy, P. J., Clarke, J. T. & Bowyer, S., 1985. *Bull. Am. astr. Soc.*, **17,** 589.

Maraschi, L., Treves, A., Tanzi, E. G., Mouchet, M., Lauberts, A., Motch, C., Bonnet-Bidaud, J. M. & Phillips, M. M., 1984. *Astrophys. J.*, **285,** 214.

Mukai, K. & Charles, P., 1985. *Mon. Not. R. astr. Soc.,* **212,** 609.
Nousek, J. A., Takalo, L. O., Schmidt, G. D., Tapia, S., Hill, G. J., Bond, H. E., Grauer, A. D., Stern, R. A. & Agrawal, P. C., 1984. *Astrophys. J.,* **277,** 682 (N84).
Oke, J. B., 1974. *Astrophys. J. Suppl.,* **27,** 21.
Osborne, J. *et al.*, 1986. *Mon. Not. R. astr. Soc.,* **221,** 823 (Paper I).
Patterson, J., 1984. *Astrophys. J. Suppl.,* **54,** 443.
Raymond, J. C., Black, J. H., Davis, R. J., Dupree, A. K., Gursky, H., Hartmann, L. & Matilsky, T. A., 1979. *Astrophys. J.,* **230,** L95.
Seaton, M. J., 1978. *Mon. Not. R. astr. Soc.,* **185,** 5P.
Szkody, P., Liebert, J. & Panek, R. J., 1985. *Astrophys. J.,* **293,** 321.
Young, P. & Schneider, D. P., 1981. *Astrophys. J.,* **247,** 960.